Bull. Mater. Sci. (2021)44:50
https://doi.org/10.1007/s12034-020-02346-6

Synthesis of Cu–Ti thin film multilayers on silicon substrates

A TORRISI[1,*], P HORÁK[1], J VACÍK[1], V LAVRENTIEV[1], A CANNAVÒ[1], G CECCIO[1], J VANIŠ[2], R YATSKIV[2] and J GRYM[2]

[1]Nuclear Physics Institute, 25 068 Husinec-Řež, Czech Republic
[2]Institute of Photonics and Electronics, 182 51 Prague, Czech Republic
*Author for correspondence (torrisi@ujf.cas.cz)

MS received 8 July 2020; accepted 11 October 2020

Abstract. Metal-oxide-based sensors (MOS) can be used for several technological applications in microelectronics, due to their low cost and sensitive capabilities to different chemical species. On the perspective to develop CuO–TiO_2 MOS, our goal was to obtain a homogeneous intermixing of Cu and Ti in the bulk structure of the detectors, exploring the most promising combination between such elements and avoiding the presence of Cu–Ti–O compounds. To do that, several Cu and Ti thin layers were alternatively deposited by Ar^+ sputtering on silicon wafers and, subsequently, oxidized by thermal annealing. The obtained samples were characterized in terms of %at. Cu–Ti ratios (by RBS and SIMS analyses) and morphology (by AFM and SEM investigations), showing the abundance ratios of such elements in the whole structure. In particular, SIMS maps allowed to study the spatial distribution and thickness of each phase of the Cu–Ti multilayers and further to observe the Cu diffusion and the mixing with Ti, as well as phase separation of CuO and TiO_2 in the samples. This unwanted effect represents an open issue that has to be investigated, in order to improve the MOS fabrication.

Keywords. Chemiresistors; Cu–Ti; intermixing layers; thermal annealing; SIMS analysis.

1. Introduction

Thin-film heterostructures can be employed in chemiresistors, which consist of electronic devices capable of changing their resistance depending on the chemical signal input (for instance detecting chemical species in gas environment). Detectable gases can extract or release electrons from/to the chemiresistor sensitive layer [1–4]. In particular, oxide heterostructures CuO–TiO_2, due to the combination of different properties of *n*-type (TiO_2, bandgap 3.0–3.2 eV) [5,6] and *p*-type (CuO, bandgap 1.2–1.5 eV) [7–9] semiconductors improve the detection limit and selectivity to certain specific gases, increasing the sensitivity to the surface-adsorbed species in comparison with conventional materials [10–13]. CuO–TiO_2 heterostructures possess high photocatalytic efficiency for selective aerobic photo-oxidation of compounds, such as methanol (CH_3OH) or methyl formate ($C_2H_4O_2$) [14], and are strongly sensitive to hydrogen, nitrogen dioxide (NO_2), acetone (C_3H_6O) and ethanol (C_2H_5OH) gas concentration [15]. Further, the structures can be employed for photocatalytic conversion of CO_2 into methane under solar irradiation [16]. They can also become promising materials for optoelectronics and competitive solar cells construction [17]. To be properly employed, the chemiresistor structure should be formed by intermixed separate CuO–TiO_2 [18] in order to create a *p*–*n* heterojunction system, increasing the overall sensitivity of the film. The aim of this study consists on the preparation of uniform CuO–TiO_2 intermixed structures, at different %at. Cu–Ti ratios, of the individual phases for successive optimization of chemiresistors. The films were subsequently annealed in air to oxidize the films and intermixing the thin layers. As a result, several multilayers with oxidized Cu and Ti phases were prepared, however with several obstacles. The most problematic is the separation of CuO from TiO_2, as well as the diffusion of Cu into the Si substrate, which remains a problem of methodology for achieving of optimized distribution of oxidized phases in the multilayer, i.e., obtaining a uniform intermixing as our final goal. The preliminary obtained results, including the analysis of the quality of the obtained films, employing several spectroscopic and microscopic techniques, will be presented and discussed.

2. Experimental

The deposition of Cu–Ti thin layers in silicon substrates (100), 1 cm^2 of area and 525 ± 20 μm each was performed by ion beam sputtering, employing as a target 99.995% pure Ti and 99.99% pure Cu foils (both from Mateck GmbH, Germany). The sputtering foils were fixed on a rotatable target holder and bombarded by a 25 keV Ar^+ (99.995%, SIAD Czech Limited) ion beam. The ion source

Published online: 25 February 2021

employed for the deposition was a Duoplasmatron of a von Ardenne type [19], which was equipped with a power supply system with a high processing stability. The Ar^+ ion current was I_i = 400 μA, the maximum time of sputtering/deposition $t \sim 120$ min and the distance between the target and the substrate was 5–6 cm. The extraction voltage was U_E = 25 kV, working pressure $p_W = 4 \times 10^{-3}$ Pa and base pressure $p_B = 8 \times 10^{-4}$ Pa. The films were deposited at room temperature and the incident angle of the Ar^+ beam on the targets was 45°. By this technique, different multilayer samples were prepared with a total film thickness of ∼150 nm. The thickness and composition of the phases were characterized by the Rutherford Back-Scattering (RBS) method using 2 MeV alpha particle ion beam at the Tandetron 4130 MC accelerator at NPI-CAS Řež [20]. The RBS spectra were evaluated by SIMNRA code [21]. The average thickness of the resulting (as-deposited) Cu–Ti films was 800×10^{15} at. cm^{-2} (corresponding to about 150 ± 5 nm). The thin films were subsequently annealed at 400°C for 24 h in air in a quartz tube with the heating (and cooling) ramp of ∼12°C min^{-1}. The chemical composition of the samples were investigated using the C-TOF SIMS (compact time-of-flight of secondary ion mass spectrometry), TOFWERK AG (Switzerland), which allowed us to investigate the depth profile of the ultrathin layers of phases in the samples. The SIMS maps and spectra were obtained using the Ga^+ ion beam with the energy of 30 keV and current of ∼1000 pA. The TOF SIMS was scanning the area of 20 × 20 μm with a resolution of 512 × 512 (∼39 × 39 nm). SEM (TESCAN LYRA3 GM, in-beam secondary electron at 20 kV) and AFM (NTEGRA scanning probe microscope (NT-MDT) and NPJPK NanoWizard Nanooptics with BRUKER TESPA-V2 tips) were also performed, to investigate the superficial morphology of the samples.

3. Experimental results

The thin multilayer films were fabricated with the 20–80, 50–50, 90–10 Cu–Ti ratios, with, respectively, 21, 17 and 25 deposition layers. SRIM code [22] was employed to simulate the 25 keV Ar^+ ion trajectories, incident at an angle of 45°, in Cu and Ti targets, to evaluate the electronic and nuclear energy loss *vs.* the depth and to calculate the sputtering yield (removed atoms per an incident Ar^+ ion). In particular, the Ar^+ trajectory in Cu and Ti *vs.* depth (figure 1a and c, respectively) and the sputtering yield of Cu and Ti atoms *vs.* their energy (figure 1b and d) were evaluated. The simulations show a sputtering yield of 14.7 (at./ion) for Cu and of 4.0 (at./ion) for Ti (figure 1b and d, respectively). Such yield was used to calculate the deposition time for each layer deposited on the silicon substrate.

Figure 2 depicts AFM images of a not-annealed sample, with a %at. 50–50 stoichiometry, scanning the square-like surface areas of (a) 2000 and (b) 500 nm^2.

It is possible to observe that the surface of the deposited films shows high uniformity of the deposited metals consisting of grains, in which size depends on the thermal annealing process (generally of about 10–100 nm in diameter), as it is possible to observe in figure 3b and d. Some larger grains (hundreds of nm) may, however, hinder the interdiffusion and mixing of the Cu and Ti phases at the employed temperature. As a peculiar example, figure 3 shows SEM (a, c) and AFM (b, d) images for %at. 90–10 (a, b) and %at. 20–80 (c, d) Cu–Ti stoichiometry, after the thermal annealing at 400°C for 24 h.

The RBS analyses of the films were performed employing 2.0 MeV alpha particles detected at 160° backscattering angle using a 50 mm^2 surface barrier Si detector and an energy-calibrated electronics. Figure 4 shows three typical spectra obtained for three different Cu–Ti ratios (%at.) before the annealing: the 20–80 (a), 50–50 (b) and 90–10 (c).

In the RBS spectra the Cu and Ti yields, corrected for the alpha energy loss in the target [23], correspond to the expected phase stoichiometry. As it is possible to observe, the Ti concentration is proportional to the oxygen concentration, whose concentration is minimal in figure 4c, where the %at. of Ti is only 10%. Such results are also confirmed by the TOF–SIMS analysis. The SIMS spectra allowed us to estimate the depth distribution of C, O and Ti in the CuO/TiO_2 structure. The SIMS images in figure 5 show, in false colour (the corresponding colour scale is shown laterally), the phase distribution of the as-deposited sample. The simultaneous presence of Cu–Ti–O combination (a), the only presence of Ti (b) and the presence of Ti–O (c) observed on the surface (top) and in the cross-section of the sample (down). In particular, figure 4b shows that the Ti concentration is higher near the surface; then, the SIMS cross-section image (figure 5e) allows to localize the Cu–Ti multilayer, in which the Ti phase is alternating with the Cu phase. Moreover, an oxidized area in proximity of the Si substrate, can also be observed, which is probably due to presence of a thin SiO_2 coating of the Si wafer.

The related SIMS depth profile spectra allow us to observe how the phases are distributed in the multilayer. It has to be taken into account that all the reported measurements, given in nm, are only qualitative and relative between the analysed phases. Figure 6 reports a typical SIMS spectrum of the detected mass-to-charge ratio yield (a) and a depth profile of the phases (b) in a not-annealed sample. In this case, the stoichiometry corresponds to the Cu–Ti %at. of 20–80 ratio, showing a film thickness well defined by the substrate Si signal, of about 60 nm, having a significant content of TiO.

Looking at the 20–80 (Cu–Ti %at.) sample in the SIMS images (figure 7a–f) and at the depth profiles (figure 7g), one can see that, after thermal annealing (400°C, 24 h), there is a higher concentration of Ti on the surface (Ti segregation up to 50 nm in depth) and a several times

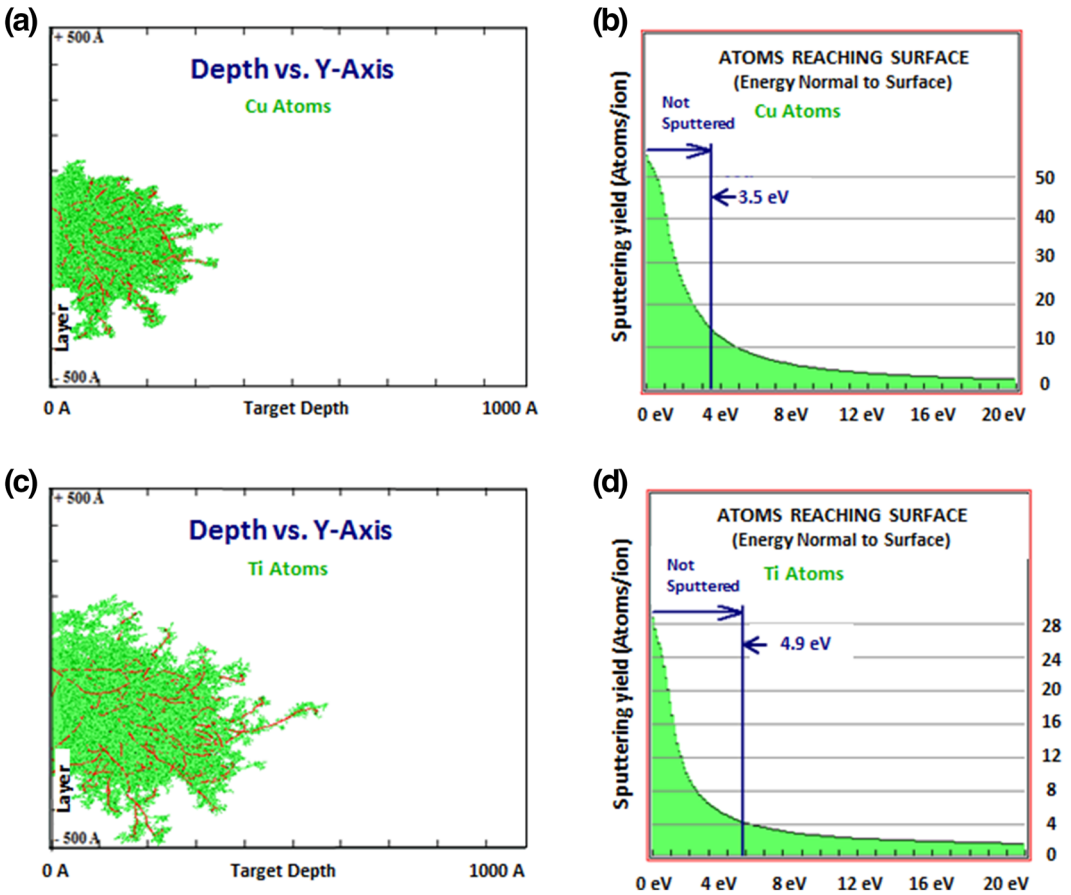

Figure 1. SRIM simulations [22] showing the Ar trajectory in (**a**) Cu and (**c**) Ti and the relative sputtering yields (**b**, **d**) for an incidence angle of 45°.

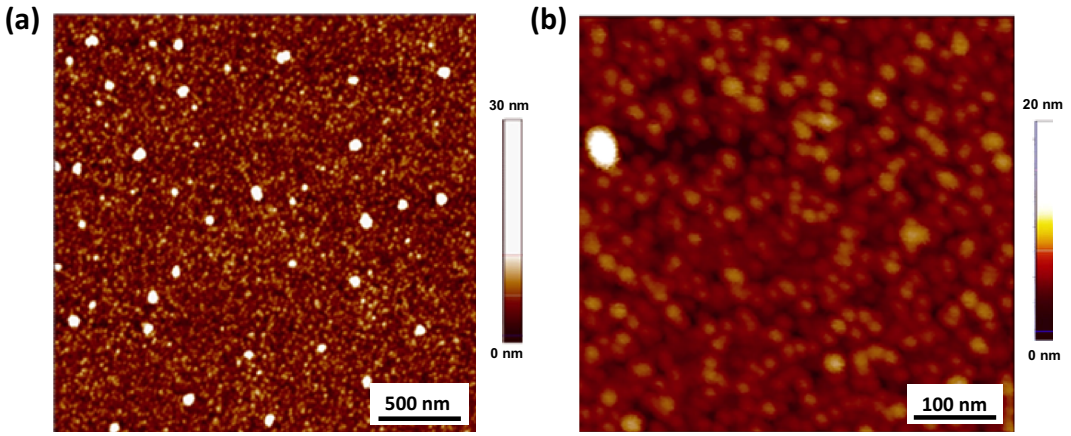

Figure 2. AFM images of a not-annealed sample having Cu–Ti stoichiometry with %at. 50–50 stoichiometry, scanning the square-like surface areas of (**a**) 2000 nm^2 and (**b**) 500 nm^2.

smaller concentration of Ti beneath, towards the Si substrate (figure 7e). Further, TiO phase follows, though with a lower concentration, the distribution of Ti (figure 7g) suggesting that only a part of Ti in the multilayer was oxidized. Figure 7a and c indicates a smaller concentration of Ti and Cu phases at the surface, due to the surface oxidation, and a higher concentration of TiO as a result of Ti oxidation due to the thermal annealing in air and not in a vacuum or in an inert gases. In the depth of about 60 nm also a small intrusion of Cu can be observed, though the reason is not clear. The cross-section in figure 7d and f confirms that only a very thin initial surface layer of the sample, less than 25 nm thick, has a high concentration of Cu and Ti.

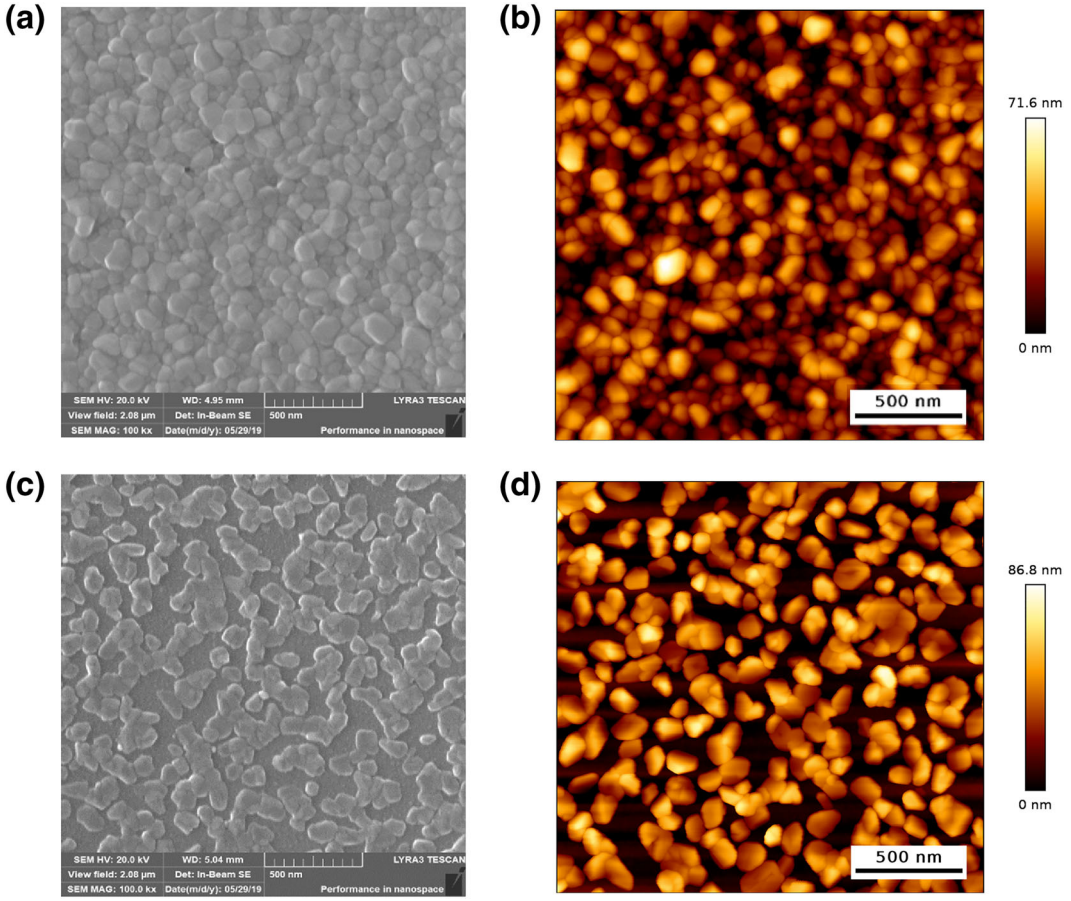

Figure 3. SEM (**a**, **c**) and AFM (**b**, **d**) images for the Cu–Ti stoichiometry %at. 90–10 (**a**, **b**) and %at. 20–80 (**c**, **d**) after the thermal annealing at 400°C for 1 h.

Figure 8 shows a similar analysis for the intermixed phase Cu–Ti in ratio 90–10. In this case, the Cu layer is present in the first 25 nm surface depth and the Ti in the range 25–150 nm depth. A Cu–Ti intermixing is detected up to the depth of about 40 nm, as a result of thermal annealing. However, the thermal processing also leads to the formation of a TiO phase at a higher concentration in a part of the Cu–Ti intermixed zone, and smaller concentration in deeper layers beneath up to about 150 nm depth.

A similar situation is also observed for the sample with the Cu–Ti ratio 50–50, as can be seen in the SIMS images (figure 9a–f) and the corresponding depth profiles (figure 9g). In this case, however, the Cu–Ti intermixing, caused by the thermal annealing, is shifted towards the surface, maintaining the thickness of about 30 nm only with a decline on the top surface layer of about 10 nm thick. Also, in this case, the maximum of the TiO phase concentration is present in the Cu–Ti intermixing zone and continues up to 150 nm depth, but with a lower concentration with respect to the previous case (figure 8) because the Ti concentration is low.

Samples prepared with other Cu–Ti ratios were annealed at the same temperature conditions (400°C, 1 h) and environment (air, 1 atm), giving responses comparable to those presented in figures 7, 8 and 9. Figure 10a shows the different SIMS curves for Cu–Ti intermixing obtained using the above described deposition and thermal annealing processing. The plot shows the depth profiles of Cu and Ti by changing the stoichiometry of the multilayers and, for comparison, the profile of the as-deposited Cu+Ti mixed films (labelled in the plot as 'Ref.'). It indicates that increasing the Cu concentration from 20% up to 90%, the Cu–Ti intermixing zone slowly enhances. Its thickness, in fact, increases from about 10 nm for 20% Cu up to about 40 nm for 90% Cu concentration. This linear growth of intermixing Cu–Ti phase with the rising of the Cu concentration is reported in the plot of figure 10b. Here it is plotted with FWHM of the Cu–Ti curves as a function of the different Cu–Ti stoichiometry ratio (in *y* axis is the standard errors of about ±3%). The result is confirmed also by the TOF SIMS data. The annealing process of Cu and Ti layers at 400°C, in air, mainly produces CuO and TiO_2 as separate compounds with a negligible presence of other oxides ($CuTiO_3$, Cu_3TiO_3 and Cu_3TiO_4), considered as an admixture, whose diffraction patterns may overlap with CuO and TiO_2, as already observed from XRD analyses, published in our previous study [13]. Moreover, as reported in refs [24] and [25], other structures as CuO_2 and $CuTiO_2$, which have not

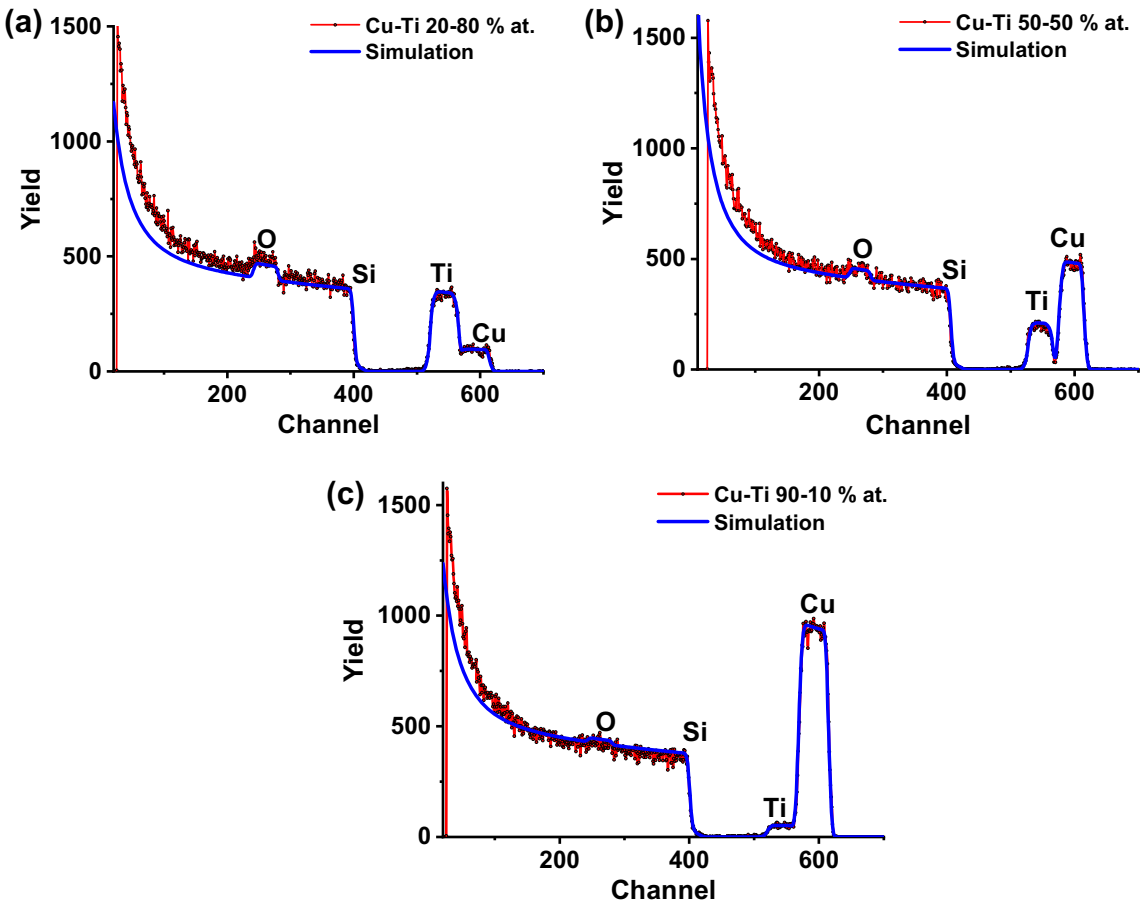

Figure 4. RBS spectra of the Cu–Ti %at. (**a**) 20–80, (**b**) 50–50 and (**c**) 90–10 samples. The simulations were performed employing the SIMNRA code [21].

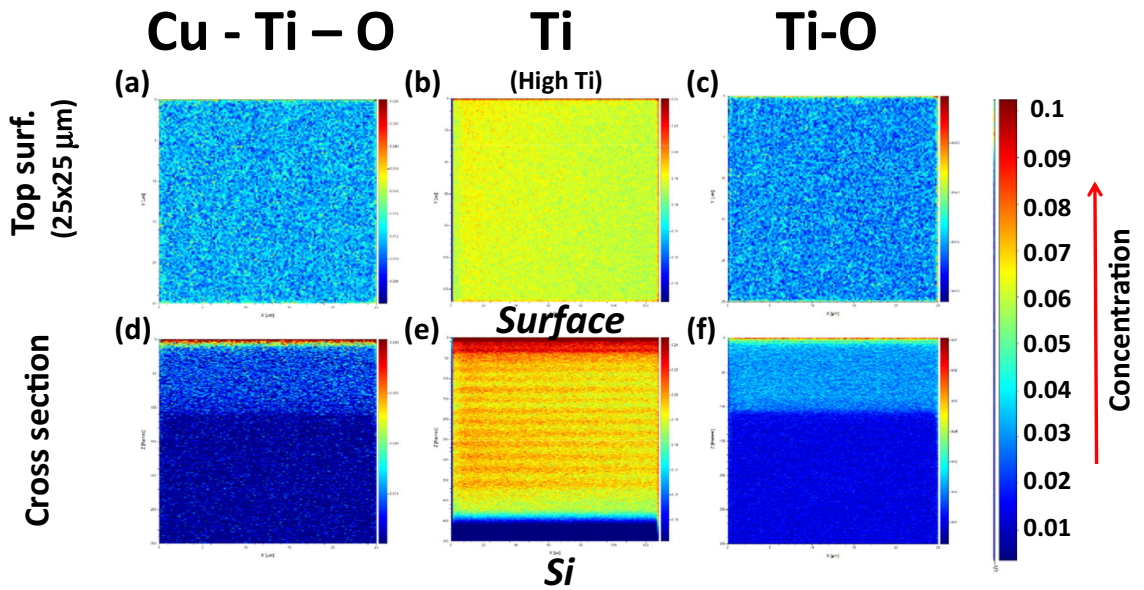

Figure 5. SIMS maps of the not-annealed Cu–Ti sample showing in false colours the concentration of Cu–Ti–O, Ti and Ti–O on the surface (**a**, **b**, **c**, respectively) and in the cross-section (**d**, **e**, **f**, respectively).

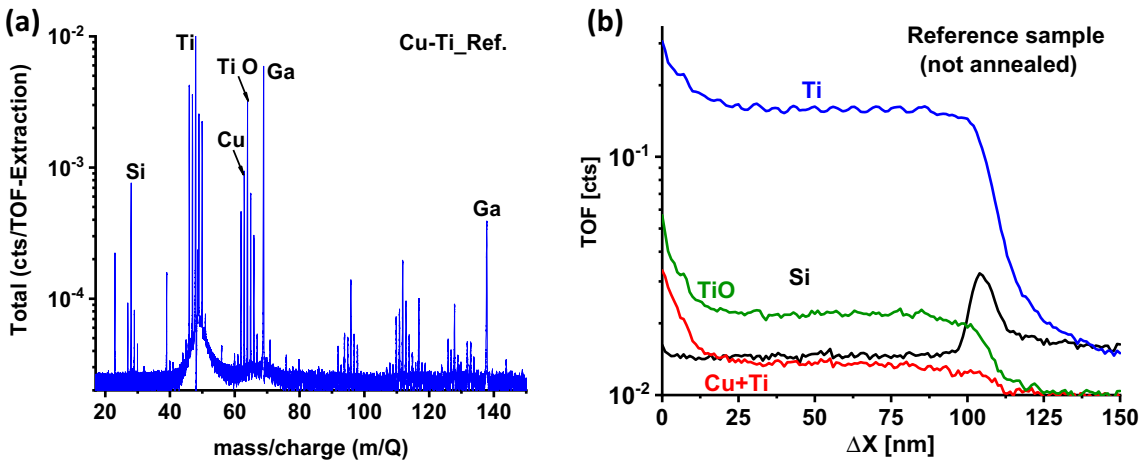

Figure 6. (**a**) TOF and (**b**) SIMS spectra for the not-annealed Cu–Ti sample.

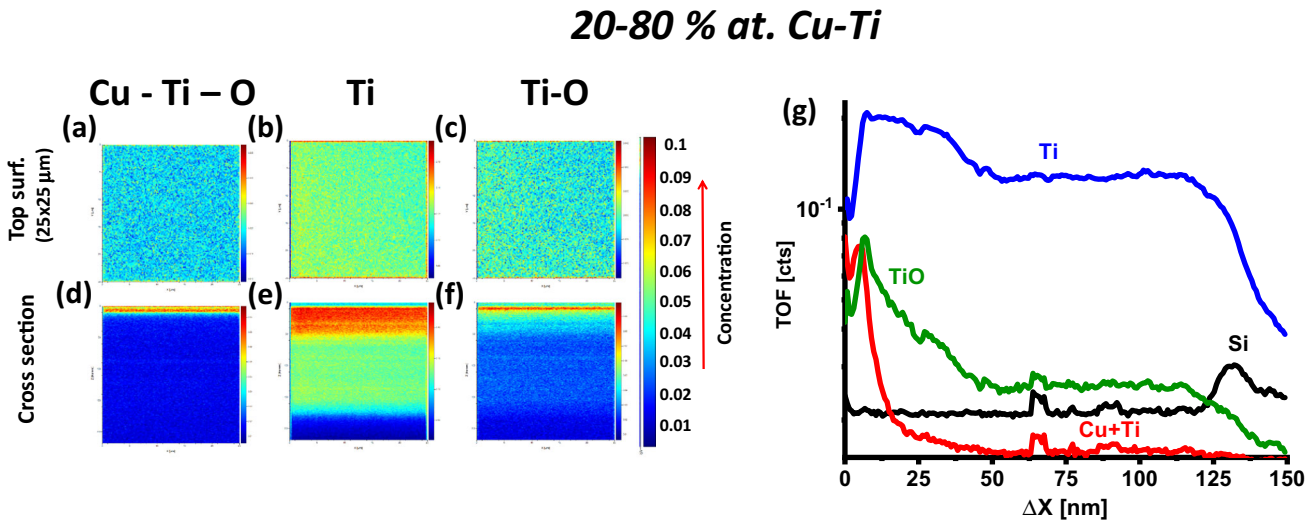

Figure 7. SIMS maps of the Cu–Ti %at. 20–80 sample showing in false colours the concentration of Cu–Ti–O, Ti and Ti–O on the surface (**a**, **b**, **c**, respectively) and in the cross-section of the sample (**d**, **e**, **f**, respectively). (**g**) Shows the related SIMS spectra of the sample.

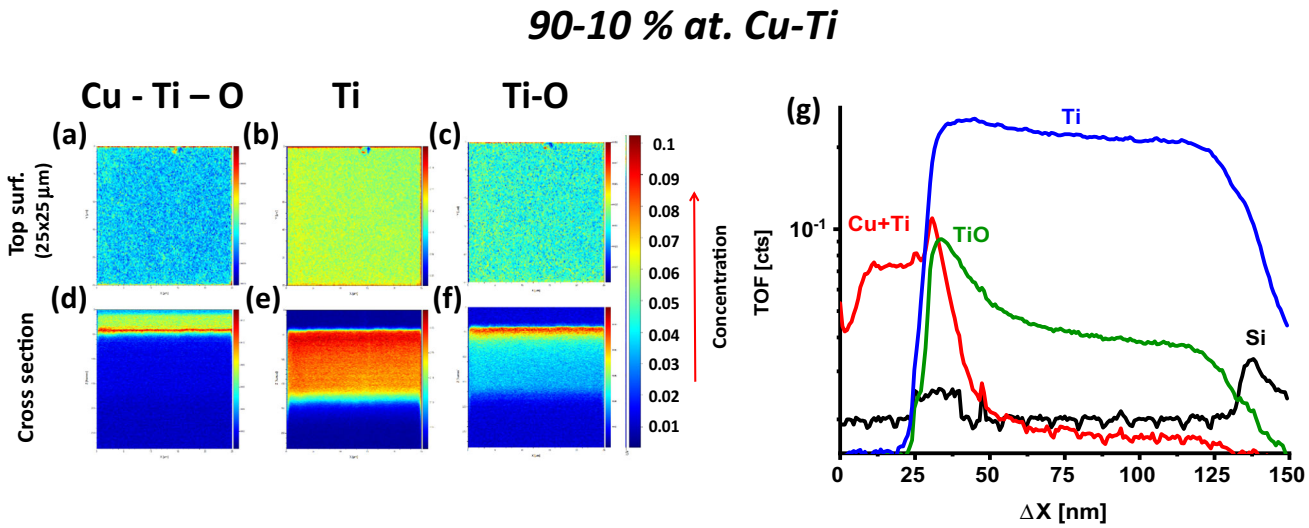

Figure 8. SIMS maps of the Cu–Ti %at. 90–10 sample showing in false colours the concentration of Cu–Ti–O, Ti and Ti–O on the surface (**a**, **b**, **c**, respectively) and in the cross-section (**d**, **e**, **f**, respectively). (**g**) Shows the related SIMS spectra of the sample.

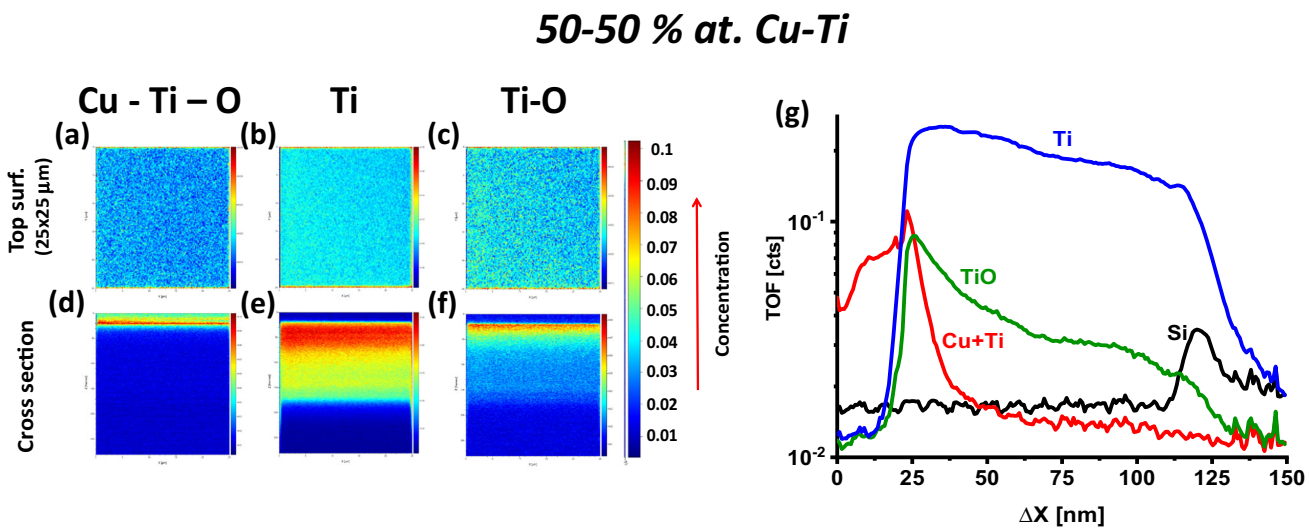

Figure 9. SIMS maps of the Cu–Ti %at. 50–50 sample showing in false colours the concentration of Cu–Ti–O, Ti and Ti–O on the surface (**a**, **b**, **c**, respectively) and in the cross-section (**d**, **e**, **f**, respectively). (**g**) Shows the related SIMS spectra of the sample.

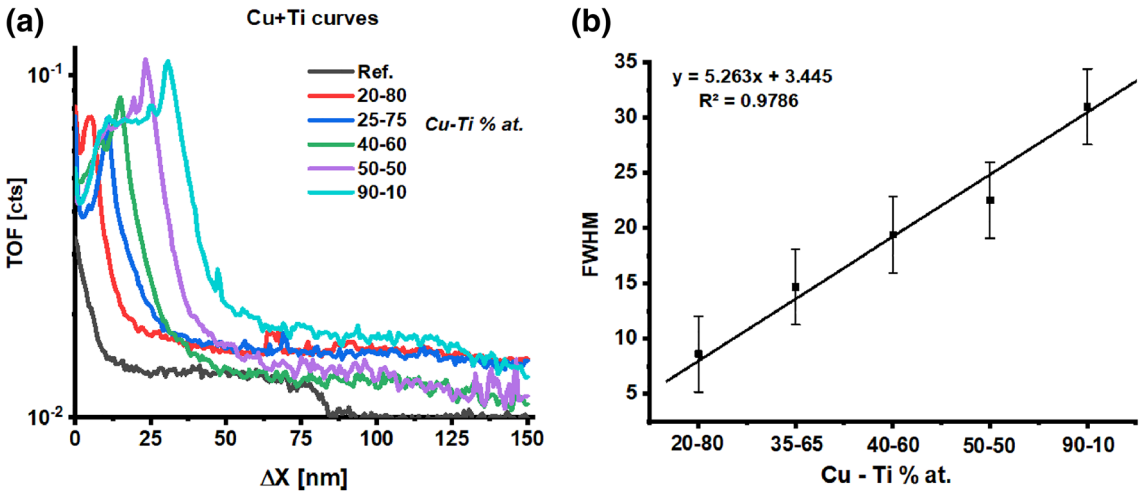

Figure 10. (**a**) Plot of the Cu+Ti curves acquired for different %at. of Cu–Ti and (**b**) FWHM distribution as a function of such values.

been found in our preliminary measurements, began evident at higher temperatures (starting from 900°C) compared to those employed for our annealing.

4. Conclusions

Thin Cu–Ti films were prepared by the ion beam sputtering technique as a preliminary investigation for the development of thin film chemiresistors. Subsequent annealing in air at 400°C led to the oxidation and formation of the oxide compound films. During the thermal annealing, mainly CuO and TiO_2 phase were formed; however, possible Cu–Ti–O compounds cannot be rejected, but their concentration does not exceed few % of the film mass. The SIMS analysis showed that during the production process a phase separation (unwanted for the gas sensing measurements) of the Cu and Ti phases also occurs and the intermixed film consists of large CuO top and TiO_2 bottom parts. The relatively narrow Cu–Ti intermixed zone is attributed to various causes, such as formation of (10–100 nm) large grains on the sample surfaces, low temperature of annealing (should be increased), annealing in air (should be performed in vacuum or in inert gas), and the presence of TiO which prevent Cu–Ti intermixing. One of the main reasons of the non-uniform intermixed Cu–Ti zone can be related to the presence of oxygen during the thermal annealing and to consequent formation of TiO layers, which act as a barrier diffusion at the sample surface. It should be avoided using the thermal processing of the as-deposited multilayers in vacuum or in inert gases first, then after intermixing also in air (or oxygen). Also the dependence from the temperature

plays an important role in the lower concentration of other compounds and in the microstructure of hot-deformed Cu–3Ti alloys, which we are going to study. Future experiments will be performed annealing the samples under vacuum or under inert gases environment, because we believe that in environment without oxygen the interdiffusion of Cu–Ti can be significantly improved. Thus, further investigations will be conducted in order to fully avoid the separation process, to induce an efficient phase intermixing and to achieve required phase oxidation in order to obtain a well intermixed CuO–TiO_2 films exhibiting an improved gas sensing performance.

Acknowledgements

This research was carried out at the CANAM infrastructure of the NPI CAS Řež (www.ujf.cas.cz). We acknowledge the financial support from the Grant Agency of the Czech Republic, Project GACR No. 19-02804S.

References

[1] Lange U and Mirsky U M 2011 *Anal. Chim. Acta* **687** 2
[2] Franke M E, Koplin T J and Simon U 2006 *Small* **2** 1
[3] Wang C, Yin L, Zhang L, Xiang D and Gao R 2010 *Sensors* **10** 3
[4] Nunes D, Pimentel A, Gonçalves A, Pereira S, Branquinho R, Barquinha P *et al* 2019 *Semicond. Sci. Technol.* **34** 043001
[5] Kang X, Liu S, Dai Z, He Y, Song X and Tan Z 2019 *Catalysts* **9** 2
[6] Haider A J, Jameel Z N and Al-Hussaini I H M 2019 *Energy Procedia* **157** 17
[7] Zhang Q, Zhang K, Xu D, Yang G and Huang H 2014 *Prog. Mater. Sci.* **60** 208
[8] Grigore M E, Biscu E R, Holban A M, Gestal M C and Grumezescu A M 2016 *Pharmaceuticals* **9** 4
[9] Rao G N, Yao Y D and Chen J W 2009 *J. Appl. Phys.* **105** 9
[10] Yatskiv R, Tiagulskyi S, Grym J, Vaniš J, Bašinová N, Horak P *et al* 2019 *Thin Solid Films* **693** 1
[11] Joshi N, Hayasaka T, Liu Y, Liu H, Oliveira Jr O N and Lin L 2018 *Microchim. Acta* **185** 213
[12] Barreca D, Carraro G, Comini E, Gasparotto A, Maccato C, Sada C *et al* 2011 *J. Phys. Chem. C* **115** 21
[13] Torrisi A, Horák P, Vacík J, Cannavò A, Ceccio G, Yatskiv R *et al* 2020 *Mater. Today: Proc.* **33** 2512
[14] Shi Q, Ping G, Wang X, Xu H, Li J, Cui J *et al* 2019 *J. Mater. Chem. A* **5** 2253
[15] Maziarz W 2019 *Appl. Surf. Sci.* **480** 361
[16] Su-Il In Dr, Vaughn II D D and Schaak R E 2012 *Angew. Chem. Int. Ed.* **51** 16
[17] Sawicka-Chudy P, Sibiński M, Wisz G, Rybak-Wilusz E and Cholewa M 2018 *J. Phys. Conf. Ser.* **1033** 012002
[18] Torrisi A, Horák P, Vacík J, Cannavò A, Ceccio G, Vaniš J *et al* 2020 *Phosphorus Sulfur Silicon Relat. Elem.* **195** 1
[19] Horak P, Lavrentiev V, Bejsovec V, Vacik J, Danis S, Vrnata M *et al* 2013 *Eur. Phys. J. B* **86** 470
[20] http://www.ujf.cas.cz/cs/vyzkum-a-vyvoj/velke-vyzkumne-infrastruktury-a-centra/canam/laboratories/Laboratory3/
[21] https://home.mpcdf.mpg.de/∼mam/
[22] http://www.srim.org/
[23] Feldman L C and Mayer J W 1986 *Fundamentals of surface and thin film analysis* (New York: North-Holland)
[24] Wongpisutpaisan N, Vittyakorn N, Ruangphanit A and Pecharapa W 2013 *Sains Malays.* **42** 175
[25] Szkliniarz A, Szkliniarz W, Blacha L and Siwiec G 2016 *Arch. Metall. Mater.* **61** 347